Manganese Oxidation States in *Gaeumannomyces*-Infested Wheat Rhizospheres Probed by Micro-XANES Spectroscopy

Darrell G. Schulze, Tina McCay-Buis, Stephen R. Sutton, and Don M. Huber

First author: Department of Agronomy, Purdue University, 1150 Lilly Hall, West Lafayette, IN 47907; second and fourth authors: Department of Botany and Plant Pathology, Purdue University, 1155 Lilly Hall, West Lafayette, IN 47907; third author: Department of Geophysical Sciences, University of Chicago, 5734 S. Ellis Ave., Chicago 60637.

Journal article 14,442 of the Purdue Agricultural Research Station.
Work supported in part by US DOE Grant 92ER14244 (SRS).
We thank R. Turco, C. Woloshuk, and two anonymous reviewers for constructive reviews of the manuscript.
Accepted for publication 26 May 1995.

ABSTRACT

Schulze, D. G., McCay-Buis, T., Sutton, S. R., and Huber, D. M. 1995. Manganese oxidation states in *Gaeumannomyces*-infested wheat rhizospheres probed by micro-XANES spectroscopy. Phytopathology 85:990-994.

The take-all disease, caused by *Gaeumannomyces graminis* var. *tritici*, is one of the world's most damaging root diseases of wheat. It has been hypothesized that the fungus reduces the host's defense mechanism prior to invasion by catalyzing the oxidation of soluble Mn^{2+} to insoluble Mn^{4+} on the rhizoplane and in the soil surrounding the root. For the first time, a direct test of this hypothesis has been accomplished using micro–X-ray absorption near edge structure (XANES) spectroscopy to obtain information about the spatial distribution of Mn oxidation states in and around live wheat roots growing in agar infected with *G. graminis* var. *tritici*. Mn in clear agar occurred only as Mn^{2+}, whereas Mn around dark roots infected with *G. graminis* var. *tritici* was predominately present as Mn^{4+}. The distribution of Mn oxidation states clearly showed the presence of Mn^{4+}-containing precipitates in the interior of a root infected with *G. graminis* var. *tritici*. This was consistent with a map of Mn concentration that showed a relative accumulation of total Mn in the interior of the root as a result of *G. graminis* var. *tritici*-catalyzed biomineralization. Given the penetrating nature of X rays, the micro-XANES technique should be applicable to roots growing in soil, thus providing a technique to measure Mn oxidation states during pathogenesis under conditions that closely simulate the natural soil environment.

Additional keywords: nutrient interactions, resistance, root rot, *Triticum*, virulence.

Manganese chemistry plays a crucial role in the etiology of a number of economically important bacterial and fungal plant diseases (11). Examples of increased disease severity associated with reduced soil Mn availability include the take-all disease of wheat (*Triticum aestivum* L.) caused by the fungus *Gaeumannomyces graminis* (Sacc.) Arx & D. Olivier var. *tritici* J. Walker, wilt of tomato (*Lycopersicon esculentum*) caused by *Verticillium alboatrum*, blast of rice (*Oryza sativa*) caused by *Pyricularia grisea*, and common scab of potato (*Solanum tuberosum*) caused by *Streptomyces scabies* (11). Most of the evidence supporting the relationship between the Mn status of the plant and disease severity has been based on a comparison of Mn concentration in tissues of healthy versus diseased plants (11). Although there are reports associating microorganisms and the reduction of Mn with disease severity (11,14), mechanistic information, which is essential for the development of improved methods of disease control, has been lacking.

Manganese is easily oxidized and reduced in soils and biological systems and can exist in either Mn^{2+}, Mn^{3+}, or Mn^{4+} oxidation states. The Mn^{2+} ion is soluble and is the predominant form taken up from the soil by plants (5,13), whereas Mn^{4+} is essentially insoluble and precipitates as various oxide and hydroxide minerals (6,17). The behavior of Mn^{3+} in soil is poorly understood, but aqueous Mn^{3+} can be stabilized by complexation with ligands (16).

Corresponding author: D. G. Schulze
E-mail address: schulze@dept.agry.purdue.edu

Biological oxidation or reduction of Mn in soil dynamically alters Mn availability to plants. It has been hypothesized that *G. graminis* var. *tritici* reduces the host's defense mechanism prior to invasion by catalyzing the oxidation of soluble Mn^{2+} to insoluble Mn^{4+} in the soil surrounding the root (8). Although indirect evidence supports this hypothesis (1,9,10,18), it has not been tested directly because of a lack of appropriate analytical techniques. Spatially resolved information on Mn within biological samples can be obtained by a number of spectroscopic techniques. Energy dispersive X-ray analysis (EDAX) conducted with an appropriately equipped electron microscope is often used to analyze the mineral content of biological specimens (1). Although EDAX analysis provides semiquantitative concentration information, it does not provide the oxidation state information important in host-pathogen interactions, and it requires that the sample be dried and placed in a high-vacuum environment. X-ray absorption near edge structure (XANES) spectroscopy is an analytical technique with the potential for measuring Mn oxidation states directly within plants, soils, or other environmental samples. An advantage of micro-XANES spectroscopy over other spectroscopic techniques is that no sample pretreatment is needed. Thus, wet samples or live plants can be analyzed without pretreatments that might alter Mn oxidation states.

XANES analytical method. In a micro-XANES spectroscopy experiment, the sample is placed in a monochromatic (narrow energy range) X-ray beam, and the absorption of the X-rays by the sample is measured as the energy of the beam is scanned across a specific energy range. The energy range is chosen to include the binding energy of a specific electron level of the element of

interest. In the present work on Mn, the innermost, or K, electron shell with a binding energy of about 6,550 eV was used to study Mn oxidation states. When the energy of the incident X rays is below the binding energy of these electrons, very few X rays are absorbed by the sample. In contrast, when the incident energy is just above the binding energy, there is a much higher probability that X rays will eject the electrons through photoelectric interactions, and absorption of X rays by the sample is, therefore, much higher. The large increase in X-ray absorption at the onset of electron ejection is called the "absorption edge" or "absorption edge jump," and the energy at which an absorption edge occurs is characteristic of the absorbing element. Absorption by the sample can be monitored by directly measuring the intensity of the transmitted X-ray beam or by detecting secondary products of the absorption process. In the present work, the intensity of the secondary fluorescent X rays was used. A fluorescent X ray is given off by an atom when another electron in the atom refills the vacancy left by the ejected electron. Fluorescent X-ray detection generally provides much lower detection limits than measuring transmitted beam intensity and is the method of choice when the absorbing element is present at low concentrations.

The XANES spectrum is a plot of sample absorption (monitored in the current study by X-ray fluorescence) versus X-ray energy in the vicinity of the absorption edge (traditionally within 40 eV of the edge). Although in general the XANES spectrum looks like a step, in detail, the X-ray absorption is altered by the atoms in close proximity to the atom of interest. Consequently, XANES spectra typically contain ripples superimposed on the absorption edge jump. These features can extend up to 1,000 eV above the edge. The intensities and frequencies of this X-ray absorption fine-structure can provide information about the numbers and distances of the nearest and next-nearest neighboring atoms (reviewed in references 3, 4, and 21). The key characteristic of XANES with regard to the present work is that the exact energies of the absorption edge and associated spectral features vary systematically with the oxidation state of the absorbing element. This effect reflects the fact that the loss of an electron by oxidation causes the remaining electrons to be bound more tightly by the nucleus, and, therefore, greater X-ray energy is required to remove the remaining electrons. As a result, the X-ray absorption edge and related spectral features shift to a slightly higher energy with each increase in oxidation state. In principle, the oxidation state of an element can be deduced from the precise energies of the XANES spectral features.

The objective of this study was to evaluate the use of micro-XANES spectroscopy to determine the oxidation state of Mn in and around wheat roots growing in an agar matrix infested with *G. graminis* var. *tritici*. These initial experiments were conducted in agar because agar is easy to work with and the roots, fungus, and precipitates can be seen easily. The long-term goal of this work is to develop experimental approaches for studying the Mn oxidation state in and around live roots growing in soil to better understand the infection process that occurs in the field.

MATERIALS AND METHODS

Specimen preparation. Petri dishes containing neutral pH, 4% potato-dextrose agar (PDA) amended with 0, 50, or 100 μg of Mn per g added as $MnSO_4$ (Mn^{2+}) were inoculated with *G. graminis* var. *tritici* cultured on PDA at 20°C. The fungus was allowed to grow for 5 to 7 days at 20°C, after which one surface-sterilized wheat seed was planted on each agar plate and allowed to germinate and grow (Fig. 1). Control plates without *G. graminis* var. *tritici* were prepared similarly. After 2 to 7 days of growth, selected seedlings were analyzed by micro-XANES spectroscopy.

Oxidation state standards. Manganese sulfate ($MnSO_4 \cdot H_2O$) was the Mn^{2+} standard, and a synthetic birnessite ($Na_4Mn_{14}O_{27} \cdot 9H_2O$), prepared as described by Golden et al. (7), was the Mn^{4+} standard. Birnessite was chosen because it is a common Mn oxide mineral in soils (15) and because it was identified previously by X-ray diffraction in a black fungal precipitate obtained by growing *G. graminis* var. *tritici* in a nutrient broth containing $MnSO_4$ as the Mn^{2+} source (D. G. Schulze, T. McCay-Buis, and D. M. Huber, *unpublished data*).

Micro-XANES spectroscopy. XANES measurements were conducted on beam line X26A at the National Synchrotron Light Source at the Brookhaven National Laboratory, Upton, NY. The synchrotron operated at 2.5 GeV and 200 mA current; the X-ray source on X26A was a bending magnet (19). The X-ray microprobe beam line consisted of a primary aperture, a channel-cut Si(111) monochromator, an 8:1 ellipsoidal focusing mirror, and a 4-jaw slit assembly. The intensity of the incident beam was monitored with an ion chamber, and the resulting Mn K_α fluorescence signal was detected using a Si(Li) energy-dispersive detector (150-eV resolution at Mn K_α) placed at 90° to the incident X-ray beam and within the horizontal plane of the synchrotron. An optical microscope was used for viewing and positioning the sample (mounted on a motorized target assembly with 1-μm precision) in the X-ray beam. Additional technical details have been discussed previously by Bajt et al. (2). Although incident X-ray spot sizes approaching 1 μm^2 have been produced with this instrument, a spot size of about 300 × 300 μm was used to increase sensitivity.

The primary aperture was 0.2 mm high at 6 m from the synchrotron source (0.3 mm vertical by 0.15 mm horizontal) resulting in a beam divergence on the monochromator of 0.04 mrad. The corresponding energy spread due to this angular divergence was 0.9 eV. The natural line width for the Mn K_α transition is 1.2 eV (12). Together with the intrinsic Darwin width of the crystal, these energy broadening effects led to an overall energy resolution of about 1.5 eV. Thus, instrumental effects only slightly degraded the intrinsically attainable resolution.

The samples consisted of small squares (about 20 × 20 mm) of agar and roots freshly cut from a larger agar plate, carefully sandwiched between two pieces of 8-μm Kapton film and mounted in 5 × 5-cm cardboard slide mounts for insertion into the sample stage. The sample mounts were placed in a stepping motor controlled sample stage to allow positioning of any desired feature of the sample under the incident beam. More than 20 spectra were collected from nine agar plates to compare the Mn oxidation states in clear agar with Mn oxidation states in infected and uninfected roots.

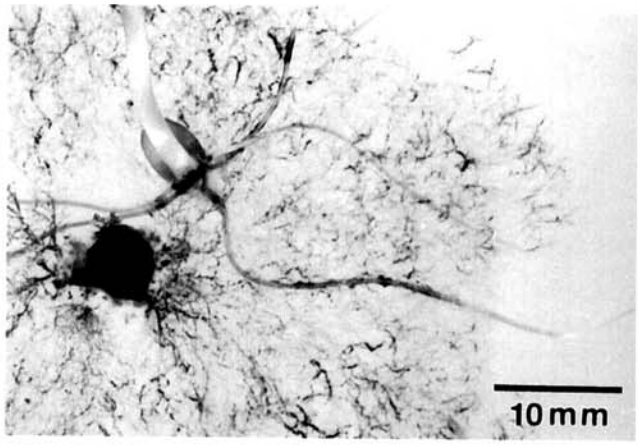

Fig. 1. A wheat seedling and the fungal root pathogen *Gaeumannomyces graminis* var. *tritici* growing on potato-dextrose agar amended with 50 μg of Mn^{2+} ($MnSO_4$) per g. The *G. graminis* var. *tritici* mycelia radiate from the dark, circular inoculum plug in the center of the dish. Dark areas along the root are sites of fungal attack. Squares of agar plus root tissue were removed from plates like this and mounted between Kapton film for micro–X-ray absorption near edge structure spectroscopy.

XANES spectra were obtained by scanning the monochromator in 0.18-eV steps over a 45-eV energy range that included the absorption edge and recording the Mn K_α fluorescence intensity at each energy step. Each energy step was counted for 2 to 10 s live time, depending on the Mn concentration of the sample, to give several-thousand counts per energy step above the absorption edge and a maximum total scan time of about 1 h for each spectrum. Energy calibration was relative to the XANES spectrum of Mn metal measured under the same experimental conditions. The half-height edge jump energy of Mn metal was assumed to be 6,539 eV.

Mapping Mn oxidation states. Maps of relative Mn^{2+} and Mn^{4+} concentrations in and around an infected root also were produced. A 15 × 15-mm square of agar containing an infected root was cut from the agar plate and mounted between Kapton film as described above. A 2 × 2-mm area, oriented so the root diagonally traversed this region, was scanned under the synchrotron beam in a raster pattern using 100-µm steps to collect three separate data sets. The first data set was collected with the monochromator tuned to 6,552.6 eV, the peak energy of absorption for Mn^{2+}. The second data set was collected with the monochromator tuned to 6,560.9 eV, the peak energy of absorption for Mn^{4+}. The third data set was obtained with the monochromator tuned to 6,615.4 eV, an energy well above the absorption edge and an energy at which the signal is due mainly to the total Mn in the sample (20). The first and second data sets were used to prepare a map of mole fraction Mn^{2+} in and around the infected wheat root, where mole fraction $Mn^{2+} = [Mn^{2+}]/([Mn^{2+}] + [Mn^{4+}])$. A calibration function derived from the intensity ratios of the Mn^{2+} and Mn^{4+} spectral peaks of dry powders of $MnSO_4 \cdot H_2O$ (the Mn^{2+} source) and a synthetic Na-birnessite (the Mn^{4+} source) (20) was used to convert the spectral data into mole fraction Mn^{2+}. An image of the distribution of total Mn in the sample (Mn^{2+} + Mn^{4+}) was prepared by plotting the absolute intensity of the third data set. Two Mn oxidation state maps, one of which is illustrated below, were prepared from two agar plates.

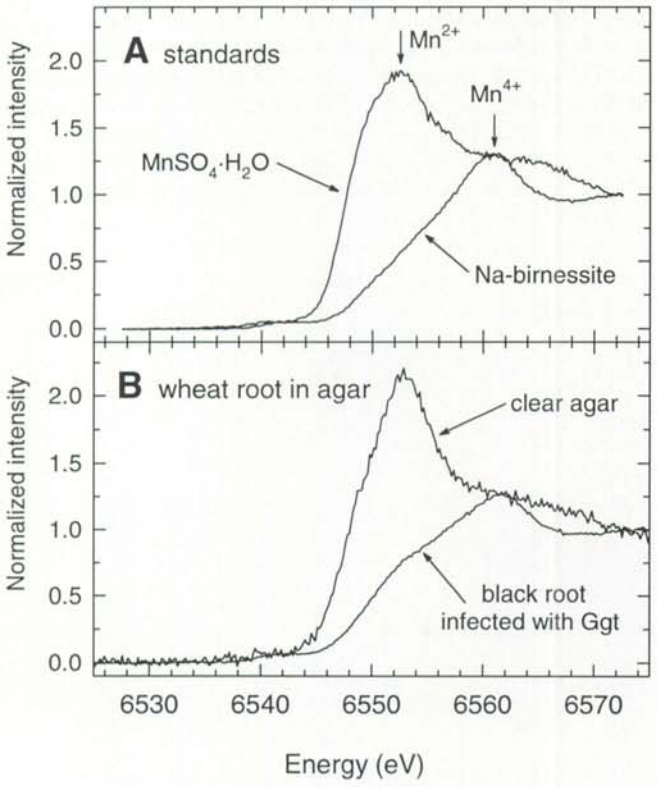

Fig. 2. Representative Mn K micro–X-ray absorption near edge structure spectra of **A,** standard mixtures containing 1,000 µg of Mn^{2+} ($MnSO_4 \cdot H_2O$) or Mn^{4+} (synthetic Na-birnessite) per g, diluted with corundum (α-Al_2O_3) and **B,** a section of wheat root infected with *Gaeumannomyces graminis* var. *tritici* (Ggt) compared with an adjacent area of clear agar.

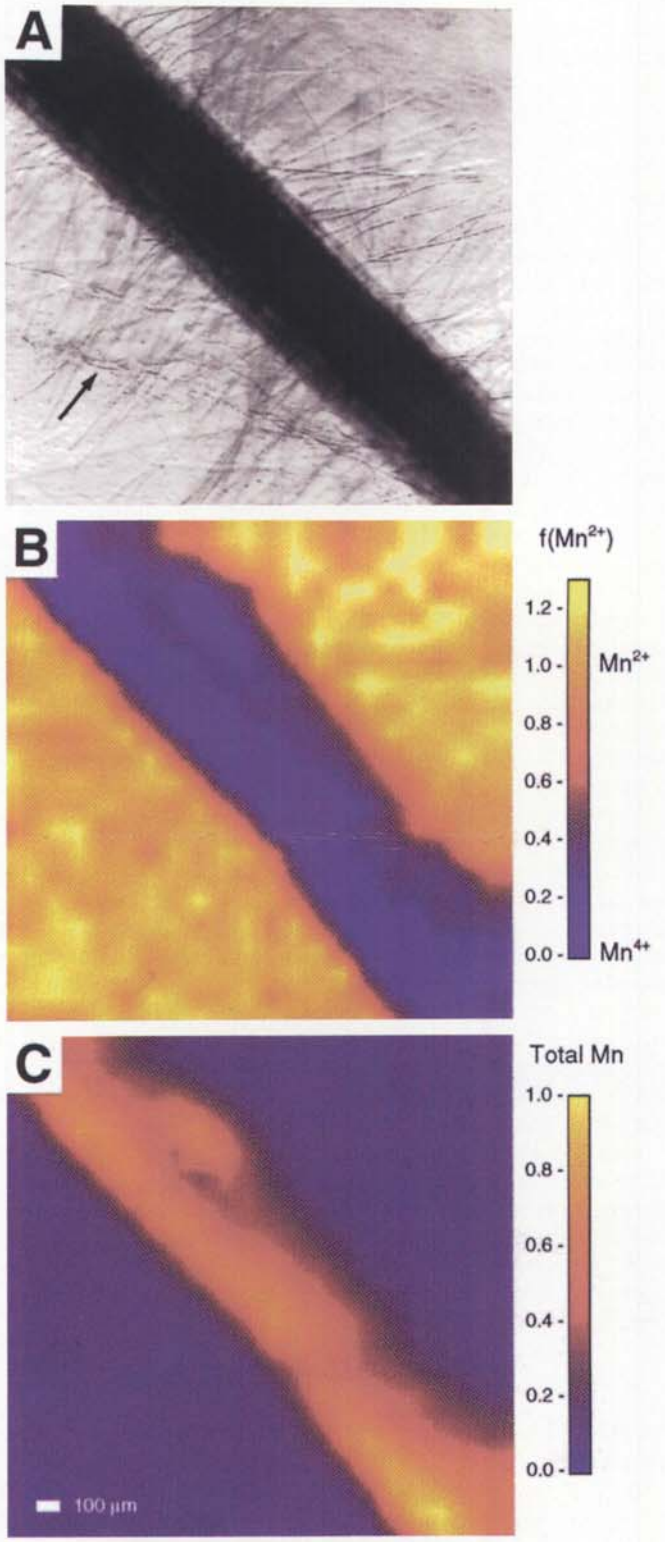

Fig. 3. A, Light microscopy image of a wheat root imbedded in potato-dextrose agar amended with 50 µg of Mn^{2+} ($MnSO_4$) per g. Arrow indicates runner hyphae approaching the root. **B,** A 2-dimensional map of the Mn oxidation state for the same area. Manganese within the agar exists primarily as Mn^{2+}, whereas Mn within the infected root is present primarily as Mn^{4+} as a result of oxidation by *Gaeumannomyces graminis* var. *tritici*. **C,** A 2-dimensional map of the relative total Mn concentration for the same area, showing the accumulation of Mn within the root. The images in **B** and **C** consist of a matrix of 21 × 21 pixels smoothed by bilinear interpolation. $f(Mn^{2+})$ = mole fraction Mn^{2+}.

RESULTS AND DISCUSSION

Agar plates that had not been amended with Mn contained too little Mn to yield useful XANES spectra and were not investigated further. The initial spectra were obtained from two agar plates containing 100 μg of Mn per g, but after it was determined that plates containing 50 μg of Mn per g yielded spectra with acceptable signal-to-noise ratios, plates containing 50 μg of Mn per g were used for the remainder of the study. The 8-eV shift in the absorption edge jump position between the spectra of the Mn^{2+} and Mn^{4+} standards made it possible to easily distinguish Mn^{2+} from Mn^{4+} (Fig. 2A). Mn in clear agar and in uninfected roots growing in Mn-amended agar occurred as Mn^{2+} as indicated by the occurrence of the absorption edge crest at 6,552.6 eV (Fig. 2B). The count rate on the fluorescence X-ray detector was proportional to the quantity of Mn present in the incident X-ray beam. Count rates indicated little or no net accumulation of Mn^{2+} by healthy roots (data not shown). Roots infected by *G. graminis* var. *tritici* were black, and the peak of the absorption edge jump occurred at 6,561.8 eV (Fig. 2B), indicating the presence of Mn^{4+}. Count rates 10 to 20 times greater than the clear agar or uninfected roots confirmed the accumulation of Mn^{4+} precipitates around the infected area of the root. This pattern of XANES spectra indicating Mn^{2+} in the clear agar and uninfected roots and Mn^{4+} in the dark, *G. graminis* var. *tritici*-infected roots was similar for each of the agar plates investigated.

Oxidation state mapping. A light microscopy image, obtained from the microscope attached to the XANES spectrometer, of a wheat root imbedded in PDA amended with 50 μg of Mn per g as $MnSO_4$ is shown in Figure 3A. The main root traversed the field of view from the upper left to lower right, and root hairs radiated perpendicularly from the main root. Fungal mycelia of *G. graminis* var. *tritici* approached the root from the lower left, but these mycelia were transparent and, thus, did not appear to be oxidizing Mn. This particular area of the root was not the site of fungal invasion and did not contain dark fungal mycelia (runner hyphae) in the cortical tissue around the root; however, the interior of the root was darkened, apparently due to Mn precipitation caused by the presence of *G. graminis* var. *tritici* within the root.

The oxidation state map of the same area (Fig. 3B) clearly shows the presence of Mn^{4+} precipitates in the interior of the root, apparently as a result of oxidation by *G. graminis* var. *tritici*, whereas Mn in the agar was in the reduced Mn^{2+} form. There also was an accumulation of total Mn in the interior of the root (Fig. 3C) as a result of oxidation by *G. graminis* var. *tritici*. Count rates indicated that up to 10 times more Mn was present in the interior of the root compared to the agar. There are two possible reasons for the accumulation of Mn. First, mass flow could have continually brought additional Mn^{2+} to the site where oxidation and precipitation was occurring. Second, in the absence of mass flow, the oxidation and subsequent precipitation reduced the concentration of Mn^{2+} in the immediate area, and additional Mn^{2+} was then free to diffuse along a gradient to replenish the Mn^{2+} removed by oxidation.

Mole fraction Mn^{2+}, by definition, should only vary between 0 and 1. Therefore, the presence of mole fractions that exceed 1 (Fig. 3B) requires an explanation. The data set from which Figure 3B and C were derived consisted of a 21 × 21 matrix of picture elements, or pixels, each containing an estimate of the mole fraction Mn^{2+} for a corresponding point on the sample. A histogram showing the number of pixels with a given mole fraction Mn^{2+} (Fig. 4) shows a bimodal distribution, with peaks at mole fractions 0.3 and 1.1.

The peak centered at mole fraction Mn^{2+} of 1.1 was due to the clear areas of agar containing only Mn^{2+}. This peak should occur at mole fraction Mn^{2+} of 1.0; the shift to 1.1 was the result of a matrix effect. Dry powders were used to prepare the standard mixtures for the calibration function, whereas the agar was essentially an aqueous system. Qualitative comparisons of the spectra of aqueous and solid $MnSO_4 \cdot H_2O$ (data not shown) have shown that the spectra differ in the intensities of the absorption edge jump and that this difference translates into an error in mole fraction Mn^{2+} similar in magnitude to that observed in Figure 3B.

Additional work is needed to quantify these matrix effects and to produce approaches for better quantification of oxidation state images. The scatter of ±0.2 mole fraction Mn^{2+} around the mean of 1.1 (Fig. 4) was due to statistical uncertainty. The agar contained only 50 μg of Mn per g, and under the particular experimental conditions used in this study, the areas of the image containing clear agar only yielded 300 to 500 counts when the monochromator was tuned to the Mn^{4+} peak (6,561.8 eV). An error analysis showed that if a pixel contained only 300 counts for the Mn^{4+} peak, the predicted mole fraction Mn^{2+} would vary about the mean by ±0.17 at the 95% confidence level. If a pixel contained 500 counts, the mean mole fraction Mn^{2+} would vary by ±0.13. These predicted errors are consistent with the approximately ±0.2 mole fraction Mn^{2+} scatter about the mean of 1.1 observed in our image (Figs. 3B and 4). Areas of the sample in which Mn had accumulated yielded up to 3,000 counts, and the predicted mole fraction Mn^{2+} varied by only ±0.05 due to statistical uncertainty in these areas. The peak at mole fraction Mn^{2+} of 0.3 was due to the oxidized areas of the image. The one pixel with mole fraction $Mn^{2+} = -0.1$ appears to be a statistical outlier. The observation that the oxidized pixels had a mean mole fraction Mn^{2+} of 0.3 rather than 0 indicates that the parts of the sample represented by these pixels contained mixtures of Mn^{4+} precipitate and soluble Mn^{2+}.

Black Mn^{4+} precipitates can be observed visually in agar systems, but it is difficult or impossible to visually identify the presence of small amounts of Mn precipitates in soil, particularly if the soil is already darkened by organic matter. We have demonstrated that Mn XANES spectra can be obtained from air-dried or moist soils containing about 700 μg of Mn per g sampled from field plots used for take-all research (20). We also have shown that if aqueous Mn^{2+} (as $MnSO_4$) is added to oxidized, air-dried soil in an amount equivalent to the total soil Mn already present, then the XANES spectrum from the soil slurry shows an increase in the intensity of the Mn^{2+} peak (C. Rottenberger and D. G. Schulze, *unpublished data*). Thus, the adaptation of the XANES techniques described above to roots growing in soil should be relatively straightforward. One potential problem, however, is that the fraction of Mn in the rhizosphere that actually participates in redox reactions may be small relative to the total soil Mn, making it difficult to detect a small change against a much larger background. If this is the case, then it may be necessary to use soils that are naturally low in total Mn. All reported biological control

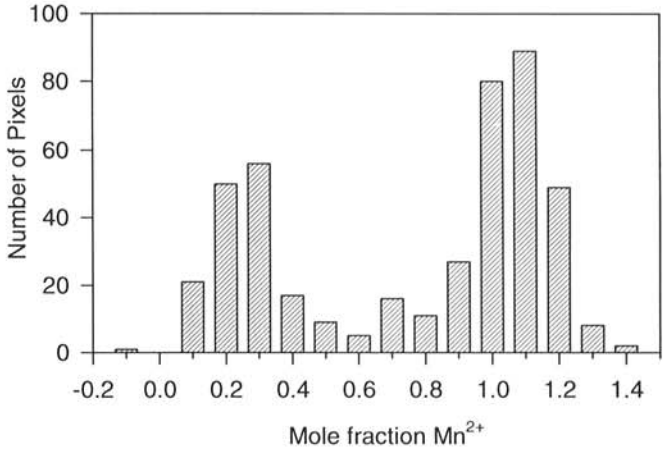

Fig. 4. Histogram showing the frequency distribution of mole fraction Mn^{2+} for the 441 individual pixels that make up Figure 3B.

organisms for take-all are strong Mn reducers in agar culture (9), but their reducing ability in soils is difficult to evaluate. The real utility of micro-XANES spectroscopy is that the Mn oxidation state in and around roots growing in soil can be studied in a natural environment. This will permit the evaluation of nutrient availability and adsorption by plants, changes in nutrient availability during the infection process, and the mechanisms by which biological control organisms influence Mn availability.

In summary, these initial results indicate that micro-XANES spectroscopy can be used to directly probe the Mn oxidation state near wheat roots infected with *G. graminis* var. *tritici*. Mn in clear agar occurred only as Mn^{2+}, whereas Mn around dark roots infected with *G. graminis* var. *tritici* was predominately Mn^{4+}. The microdistribution of the Mn oxidation states clearly showed the presence of Mn^{4+}-containing precipitates in the interior of a root infected with *G. graminis* var. *tritici*. It should be possible to use this technique to study roots growing in soil under conditions chosen to simulate field conditions. We have already demonstrated that XANES spectra of Mn in soils can be obtained at ambient Mn concentrations (20). Many spectroscopic techniques require that the sample be placed in a high-vacuum environment and require fixing and drying steps that may introduce artifacts such as changes in oxidation state or redistribution of elements in the sample. Micro-XANES spectroscopy is unique in that live roots growing in agar or moist soil can be easily studied in the presence of soilborne, root-infecting organisms or their potential biological control agents.

LITERATURE CITED

1. Arnott, H. J., Roseman, T. S., Graham, R. D., and Huber, D. M. 1991. An experimental study of manganese mineralization in the take-all fungus, *Gaeumannomyces graminis*. Mycol. News 42:3.
2. Bajt, S., Clark, S. B., Sutton, S. R., Rivers, M. L., and Smith, J. V. 1993. Synchrotron x-ray microprobe determination of chromate content using x-ray absorption near-edge structure. Anal. Chem. 65:1800-1804.
3. Brown, G. E., Jr. 1990. Spectroscopic studies of chemisorption reaction mechanisms at oxide-water interfaces. Pages 309-363 in: Mineral-Water Interface Geochemistry. M. F. Hochella, Jr. and A. F. White, eds. Reviews in Mineralogy, vol. 23. Mineralogical Society of America, Washington DC.
4. Brown, G. E., Jr., Calas, G., Waychunas, G. A., and Petiau, J. 1988. X-ray absorption spectroscopy and its applications in mineralogy and geochemistry. Pages 431-512 in: Spectroscopic Methods in Mineralogy and Geochemistry. F. Hawthorne, ed. Reviews in Mineralogy, vol. 18. Mineralogical Society of America, Washington DC.
5. Clarkson, D. T. 1988. The uptake and translocation of manganese by plant roots. Pages 101-111 in: Manganese in Soils and Plants. R. D. Graham, R. J. Hannam, and N. C. Uren, eds. Kluwer Academic Publishers, Boston.
6. Dixon, J. B., and Skinner, H. C. W. 1992. Manganese minerals in surface environments. Pages 31-50 in: Biomineralization Processes of Iron and Manganese: Modern and Ancient Environments. H. C. W. Skinner and R. W. Fitzpatrick, eds. Catena Verlag, Cremlingen-Destedt, Germany.
7. Golden, D. C., Chen, C. C., and Dixon, J. B. 1987. Transformation of birnessite to buserite, todorokite, and manganite under mild hydrothermal treatment. Clays Clay Miner. 35:271-280.
8. Graham, R. D. 1983. Effect of nutrient stress on susceptibility of plants to disease with particular reference to the trace elements. Adv. Bot. Res. 10:221-276.
9. Huber, D. M., and McCay-Buis, T. S. 1993. A multiple component analysis of the take-all disease of cereals. Plant Dis. 77:437-447.
10. Huber, D. M., McCay-Buis, T. S., Graham, R. D., and Robinson, N. 1993. Cultural conditions affecting take-all and their effects on manganese availability. 6th Int. Congr. Plant Pathol. Abstr. 179. National Research Council of Canada, Ottawa, ON.
11. Huber, D. M., and Wilhelm, N. S. 1988. The role of manganese in resistance to plant diseases. Pages 155-173 in: Manganese in Soils and Plants. R. D. Graham, R. J. Hannam, and N. C. Uren, eds. Kluwer Academic Publishers, Boston.
12. Krause, M. O., and Oliver, J. H. 1979. Natural widths of atomic K and L levels, K_α x-ray lines and several KLL Auger lines. J. Phys. Chem. Ref. Data 8:329-338.
13. Marschner, H. 1988. Mechanisms of manganese acquisition by roots from soils. Pages 191-204 in: Manganese in Soils and Plants. R. D. Graham, R. J. Hannam, and N. C. Uren, eds. Kluwer Academic Publishers, Boston.
14. Marschner, P., Ascher, J. S., and Graham, R. D. 1991. Effect of manganese-reducing rhizosphere bacteria on the growth of *Gaeumannomyces graminis* var. *tritici* and on manganese uptake by wheat (*Triticum aestivum* L.). Biol. Fertil. Soils 12:33-38.
15. McKenzie, R. C. 1989. Manganese oxides and hydroxides. Pages 439-465 in: Minerals in Soil Environments. J. B. Dixon and S. B. Weed, eds. Soil Science Society of America, Madison, WI.
16. Norvell, W. A. 1988. Inorganic reactions of manganese in soil. Pages 37-58 in: Manganese in Soils and Plants. R. D. Graham, R. J. Hannam, and N. C. Uren, eds. Kluwer Academic Publishers, Boston.
17. Post, J. E. 1992. Crystal structures of manganese oxide minerals. Pages 51-73 in: Biomineralization Processes of Iron and Manganese: Modern and Ancient Environments. H. C. W. Skinner and R. W. Fitzpatrick, eds. Catena Verlag, Cremlingen-Destedt, Germany.
18. Roseman, T. S., Graham, R. D., Arnott, H. J., and Huber, D. M. 1991. The interaction of temperature with virulence and manganese oxidizing potential in the epidemiology of *Gaeumannomyces graminis*. (Abstr.) Phytopathology 81:1215.
19. Schulze, D. G., and P. M. Bertsch. 1995. Synchrotron x-ray techniques in soil plant and environmental research. Adv. Agron. 55:1-66.
20. Schulze, D. G., Sutton, S. R., and Bajt, S. Determination of manganese oxidation state in soils using x-ray absorption near-edge structure (XANES) spectroscopy. Soil Sci. Soc. Am. J. In press.
21. Teo, B. 1986. EXAFS: Basic principles and data analysis. Springer Verlag, New York.